Food Production, Processing and Nutrition

RESEARCH

Open Access

Arugula leaf nanovesicles as sustainable food ingredient: processing, stability, and bioavailability

Lorenza d'Adduzio[1], Davide Marangon[1], Umberto Musazzi[1], Giorgia Frigerio[1], Giulia Ranaldi[2], Barbara Lazzari[3], Luigi Sironi[1], Raffaele Pugliese[4], Maria Pia Abbracchio[1], Davide Lecca[1] and Carmen Lammi[1*]

Abstract

Plant-derived nanovesicles (PDVs) are emerging as natural nanostructures with potential applications in food and nutraceutical systems. In this study, we report the scalable production of arugula leaf–derived nanovesicles (ALVs) through ultrafiltration-size exclusion purification followed by spray-drying stabilization. This workflow ensured preservation of nanoscale morphology, biochemical cargo, and stability during long-term storage. Comprehensive characterization by cryo-EM, Raman spectroscopy, circular dichroism, and LC-HRMS revealed that ALVs contain amino acids, fatty acids, phenolic acids, flavonoids, and lignans, along with regulatory plant miRNAs. Importantly, ALVs were able to cross differentiated Caco-2 intestinal monolayers without compromising barrier integrity, suggesting safe oral bioavailability. Overall, this work establishes arugula-derived nanovesicles as sustainable, stable, and bioavailable food nano-ingredient, highlighting their potential integration into functional foods and nutraceutical applications.

Keywords Plant-derived nanovesicles, Arugula, Spray-drying, Stability, Bioavailability, Functional nutrition

*Correspondence:
Carmen Lammi
carmen.lammi@unimi.it
Full list of author information is available at the end of the article

Graphical Abstract

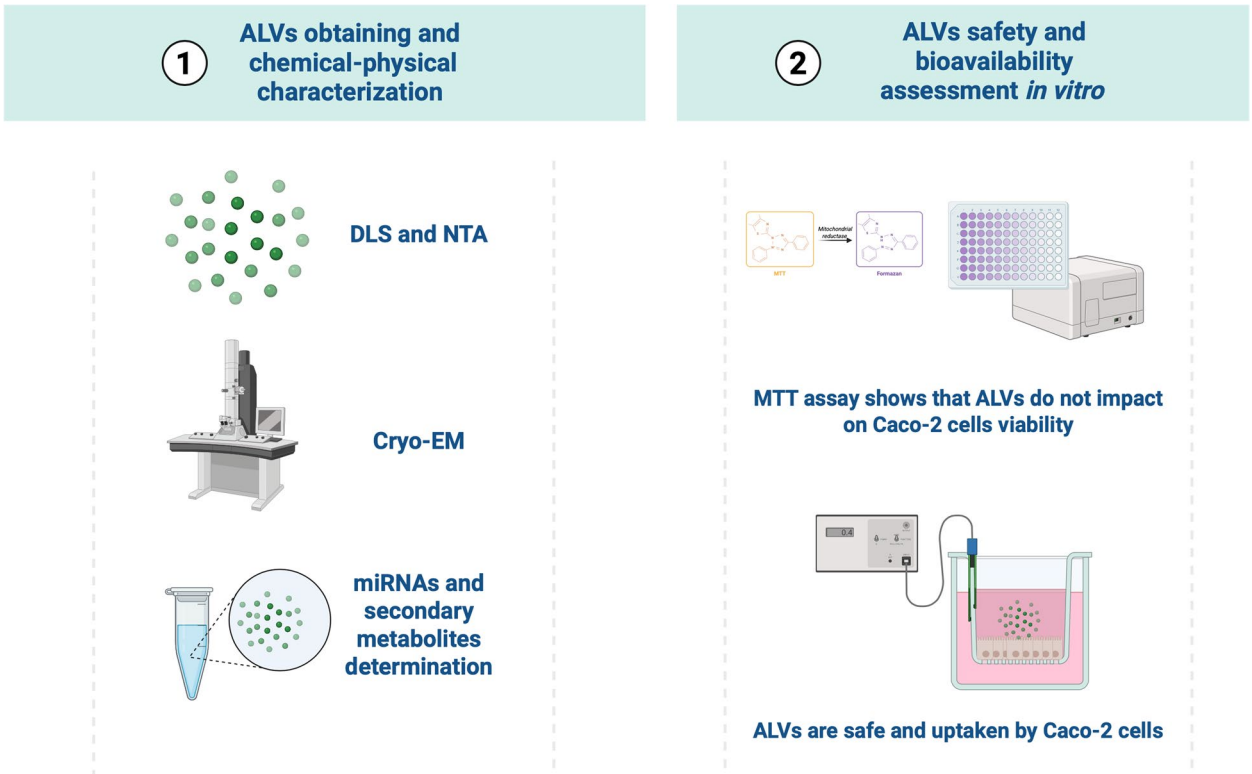

Introduction

The exploration of naturally occurring colloidal structures in foods has opened new perspectives in both fundamental and applied food science. Among these, plant-derived nanovesicles (PDVs) have recently attracted attention as self-assembled nanoscale structures originating from edible sources (S. Q. Kim & K.H. Kim, 2022). PDVs are round shaped structures having a dimeter of 30–150 nm that naturally contain many bioactive compounds that play an essential role in cell-to-cell communication, in particular lipid, proteins, genetic material (DNA, miRNAs) and metabolites (Kameli et al., 2021). PDVs can be artificially obtained during the proper plant material tissue processing, where the rearrangement of the cellular membranes induced the nanovesicles formation, so that PDVs' content reflects the phytochemical profile of the plant matrix, being naturally bioformulated carriers of bioactive compounds. These vesicles share several features with other food hydrocolloids and colloidal systems, including bilayer organization, encapsulation of bioactive molecules, and the ability to interact with biological interfaces (Tan & McClements, 2021). Their intrinsic nanoscale architecture positions them as promising candidates for stability enhancement and functional delivery of naturally occurring food components. The characterization of PDVs has revealed a complex molecular composition, comprising lipids, proteins, metabolites, and nucleic acids, which may contribute to both their structural stability and functional properties (Rome, 2019). However, their application within food and nutraceutical systems requires solutions to challenges common to colloidal delivery vehicles: scalability of production, preservation of integrity during storage, and reproducible bioavailability upon oral intake (Johnston et al., 2011; Kolluru et al., 2021). Addressing these challenges is essential for advancing PDVs from conceptual interest to practical use as food-derived nanostructures. In this context, arugula (*Eruca sativa*) leaves represent a valuable model. They are rich in phenolics, flavonoids, and glucosinolate-derived metabolites, and widely consumed as part of the human diet (Ortega-Hernández et al., 2021). Isolating nanovesicles from arugula provides not only a sustainable source of nanoscale carriers but also a food-grade system compatible with nutraceutical development. By applying scalable processes such as ultrafiltration-size exclusion purification

and spray-drying stabilization, it is possible to produce stable nanostructures while preserving their biochemical cargo and functional integrity.

The present study integrates process engineering, chemical characterization, and functional evaluation to demonstrate the potential of arugula-derived nanovesicles (ALVs) as food-based nanostructures. Specifically, we provide detailed structural and compositional analysis, assess stability during long-term storage, and investigate their behavior at key biological interfaces. More in detail, the ALVs bioavailability was evaluated in vitro on differentiated human intestinal Caco-2 cells. This work contributes to the growing field of natural hydrocolloid derived nanostructures in food science, positioning ALVs as an innovative platform for the design of advanced food hydrocolloid systems and nutraceutical carriers.

Material and methods

Materials

All chemicals and reagents were of analytical grade and from commercial sources. Ready-to-eat arugula leaves were purchased from local supermarket and stored at 4 °C until the processing. The complete list of all chemicals and reagents could be found in supplementary materials.

Arugula leaves nanovesicles obtaining, purification and stabilization

Our method for the production, purification and stabilization of plant-derived nanovesicles, comprised these following steps: homogenization of the vegetable matrix with a blender of to obtain a homogenate; separation (sieving) of the juice from the solid residue present in the homogenate obtained; isolation and purification of the nanovesicles thus obtained via ultrafiltration with two types of cut-off (100 and 10 kDa) coupled to size exclusion chromatography (SEC), using column Izon qEV Original 35 nm, collecting some specific eluted fractions stabilization of the nanovesicles and nanoparticles by spray-drying. More detailed information available in our patent (International Publication Number WO 2024/223549 A1).

Dynamic Light Scattering (DLS) Analysis

The Z-average diameter (D_h) and the polydispersity index (PDI) of samples were evaluated by photon correlation spectroscopy using a dynamic light scatter (DLS, Zetasizer Nano ZS, Malvern Instrument, Malvern, UK), equipped with a backscattered light detector, operating at dual angle (173°, 12.8°) mode and at 25 °C. More detailed information can be found in supplementary material.

Nanoparticle tracking analysis (NTA)

Particle size distribution and concentration were analyzed by a nanoparticle tracking analysis (NTA) using a NanoSight NS300 (Malvern Panalytical, Malvern, UK) equipped with a blue laser (404 nm, 70 mV) and sCMOS camera. Detailed information could be found in Supplementary material section.

Spray-drying stabilization

Aliquots of nanosuspension were diluted in a trehalose solution to obtain a final sugar concentration of 10% w/v. The obtained mixture was sprayed through a two-fluid nozzle, operating in a co-current manner, of a Format 4 M8 (ProCepT, Belgium).

According to the published results on parameter optimization (Magri et al., 2019), the process parameters were set as follows: inlet temperature = 120 °C; feed flow rate = 5.0 mL/min; nozzle pressure = 1.7 atm; nozzle diameter = 0.4 mm; $\Delta P = 70$ mbar. See supplementary materials for full details.

Morphological analysis by cryogenic electron microscopy (Cryo-EM)

Spray-dried ALVs sample was resuspended in water in saturated conditions. Sample vitrification was carried out with a Mark IV Vitrobot (Thermo Fisher Scientific). The 3 μL of sample were applied to a Quantifoil R 2/1 Cu 300-mesh grid and Lacey grids previously glow-discharged at 30 mA for 30 s in a GloQube (Quorum Technologies). Details are provided in the supplementary materials.

Raman spectroscopy

Raman analysis was conducted using Progeny TM spectrophotometer (Rigaku Corporation, Japan) with a 1,064 nm laser source, using a laser output set at 490 mW. The spectral range was at 200–2,500 cm^{-1} with transmission-type volume phase grating. The complete methodology was described in the supplementary material.

Intrinsic fluorescence analysis

The intrinsic fluorescence spectrum of each sample was obtained using a fluorescence spectrophotometer (Synergy H1, Biotek, Bad Friedrichshall, Germany). The samples were diluted in phosphate-buffered saline (PBS, 10 mM, pH 7.0) in order to reach the equal concentration of 0.05 mg/mL and transferred in Greiner UV- Star® 96 well plates flat bottom clear cyclic olefin copolymer (COC) wells (cycloolefine). More detailed information could be found in supplementary materials section.

ALV chemical composition analysis

Secondary metabolite determination by HR-HPLC–MS/MS

The extraction of polyphenols was carried out in triplicate and the entire procedure was performed in the darkness. ALVs powder was homogenized with acidified methanol (HCl 0.1% v/v) at 4% w/v. The sample was subsequently placed in an ultrasonic bath for 15 min and centrifuged at 12,500 rpm for 5 min; the pellet was discarded, and the supernatant was stored at −80 °C until analysis. Samples have been analyzed at UNITECH OMICs (University of Milano, Italy) using the ExionLC™ AD system (SCIEX connected ZenoTOF 7600 System (SCIEX) equipped with Turbo V™ Ion Source with ESI Probe. Supplementary materials contain further explanation.

miRNome determination

For total RNA extraction 100 mg ALVs powder were first dissolved in 1 mL of TRI-reagent (Zymo Research) and then vigorously mixed with 200 µl of chloroform (Sigma-Aldrich). The homogenate was centrifuged, and the upper aqueous phase containing RNA was mixed with an equal volume of 99.8% ethanol (Sigma-Aldrich) and loaded in a Zymo-Spin™ column for RNA purification (Zymo Research). Detailed information was shown in the supplementary materials (Simon Andrews, 2020; Yi et al., 2015).

ALVs Staining with Merocianine Dye 540

The 100 mg of ALVs powder was solved in H_2O sterile and Merocianine Dye 540 (Merocyanine 540, Dye content 90, Sigma-Aldrich) was added to reach the final concentration of 100 µM. The solution was incubated far from light for 60 min. To remove the excess of dye, the solution was ultracentrifuged for 3 h at 28,800 RPM in Beckman Coulter (rotor type 50.2 Ti) at 4 °C. The pellet was resuspended in TrisHCl 20 mM pH 7.2.

ALV characterization on cellular model

Cell culture conditions

Caco-2 cells were cultured in DMEM high glucose with stable L-glutamine, supplemented with 10% FBS, 100 U/mL penicillin, 100 µg/mL streptomycin (complete growth medium) with incubation at 37 °C under 5% CO_2 atmosphere (Natoli et al., 2012). Natoli et al. (2012) Further details could be found in the Supplementary material section.

3-(4,5-Dimethylthiazol-2-yl)−2,5-diphenyltetrazolium Bromide (MTT) Assay

The MTT experiments were conducted on human intestinal Caco-2 cells according previous set up conditions (d'Adduzio et al., 2024). Briefly, a total of 3×10^4 cells/well were seeded in 96-well plates and, after 24 h, treated with ALVs 0,01–1 mg/mL, or vehicle, in complete growth media for 48 h at 37 °C under 5% CO_2 atmosphere. More detailed information can be found in the Supplementary material.

Trans-epithelial Transport on Caco-2 cells

Caco-2 Cell Culture and Differentiation Human intestinal Caco-2 cells, obtained from INSERM (Paris, France), where cultured according to a published protocol (Natoli et al., 2012). For differentiation, Caco-2 cells were seeded onto polycarbonate filters (Transwell, Corning Inc., Lowell, MA, USA) with a 12 mm diameter and 0.4 µm pore size, at a density of 3.5×10^5 cells/cm^2. The cells were cultured in complete medium containing 10% FBS in both the apical (AP) and basolateral (BL) compartments for 2 days to allow the formation of a confluent monolayer. (Ferruzza et al., 2013). Additional information could be found in the supplementary information.

Cell monolayers integrity evaluation The transepithelial electrical resistance (TEER) of differentiated Caco-2 cells was measured at 37 °C using the voltmeter apparatus Millicell (Millipore Co., Billerica, MA, USA), immediately before and at the end of the transport experiments. The complete methodology is described in the supplementary file.

Trans-epithelial transport assessment Prior to experiments, the cell monolayer integrity and differentiation were checked by TEER measurement as described in detail above. Merocyanine 540-labeled ALVs trans-epithelial passage was assayed in differentiated Caco-2 cells in transport buffer solution according to previously described conditions (Lammi et al., 2021). See supplementary materials for full details about the methodology.

Morphological analysis of Caco-2 cells by Confocal Microscopy After 2 h incubation in the absence or in the presence of 8×10^6 or 40×10^6 labeled ALVs/mL in the Apical compartment, cells where washed and fixed with 2% paraformaldehyde 30 min at RT. Supplementary materials contain further explanation.

Statistical analysis

All the Data set were checked for normal distribution by D'Agostino & Pearson test. Since they were all normally disturbed with p-values < 0.05, we proceeded with statistical analyses by One-Way ANOVA followed by Dunnett's and Tukey's post-hoc tests and using Graphpad Prism 9 (San Diego, CA, USA). Values were reported as means ± s.d. or SEM (in the case of in vivo study); p-values < 0.05 were significant.

Results

ALVs: Production and Chemical characterization

ALVs: Production and stabilization

In this study, we developed an efficient method to obtain PDVs while preserving their structure and morphology. Size exclusion chromatography (SEC), coupled to ultrafiltration (UF) was applied to produce purified sample. The ALVs obtained with the proposed innovative method showed a narrow particle size distribution in the nanoscale range. By combining dynamic light scattering (DLS) in dual-angle mode and nanoparticle tracking analysis (NTA) we could better evaluate the purification methods' effectiveness and detect aggregates. Samples purified with UC showed higher size compared to those processed using UF/SEC purification when analyzed using both DLS and NTA (Fig. 1; Table 1). As reported in Table 1, ALVs extracted using UC were highly polydisperse at DLS (PDI > 0.5), indicating the presence of heterogeneous material in the sample. Aggregates detected at 12.8° (Table 1) and by the NTA (Fig. 1) further confirmed that UC is not suitable to obtain reproducible and stable ALVs. Conversely, UF/SEC purification slightly reduced particle concentration in comparison to UC-purified samples but resulted in vesicles with a smaller particle size and narrower PDI. Consequently, UF/SEC was selected over UC for purifying ALVs and assessing the impact of spray-drying on vesicle stability. As reported in Table 1, the spray-drying process did not affect ALVs' size distribution or concentrations. The D_h of resuspended dried powder remained comparable to the pre-spray drying values ($D_{h,f}/D_{h,i} = 0.9$) with no aggregates detected by either DLS or NTA. These results highlighted the impact of purification methods on ALVs' particle size distribution and concentration. Moreover, as shown in in Supplementary Table S3, ALVs retained stability in terms of vesicles concentration and 24 months of storage.

Based on these findings, the optimal protocol for obtaining enriched and stable ALV fractions combines UF/SEC purification with spray drying (Fig. 2). Cryogenic electron microscopy (Cryo-EM) analysis revealed densely filled structures measuring 0.5–2 µm with sharp, membrane like edge and of 50–200 nm structures without sharp edge, likely corresponding to lipidic droplets (Fig. 2A, B).

Physico-chemical characterization of ALVs

The ALVs obtained using UF/SEC coupled to spray drying were subjected to physico-chemical characterization through biochemical and spectroscopic techniques. The protein content of ALVs, determined by the Bradford Assay, was measured 6.25 (± 0.38) µg/mL. To explore

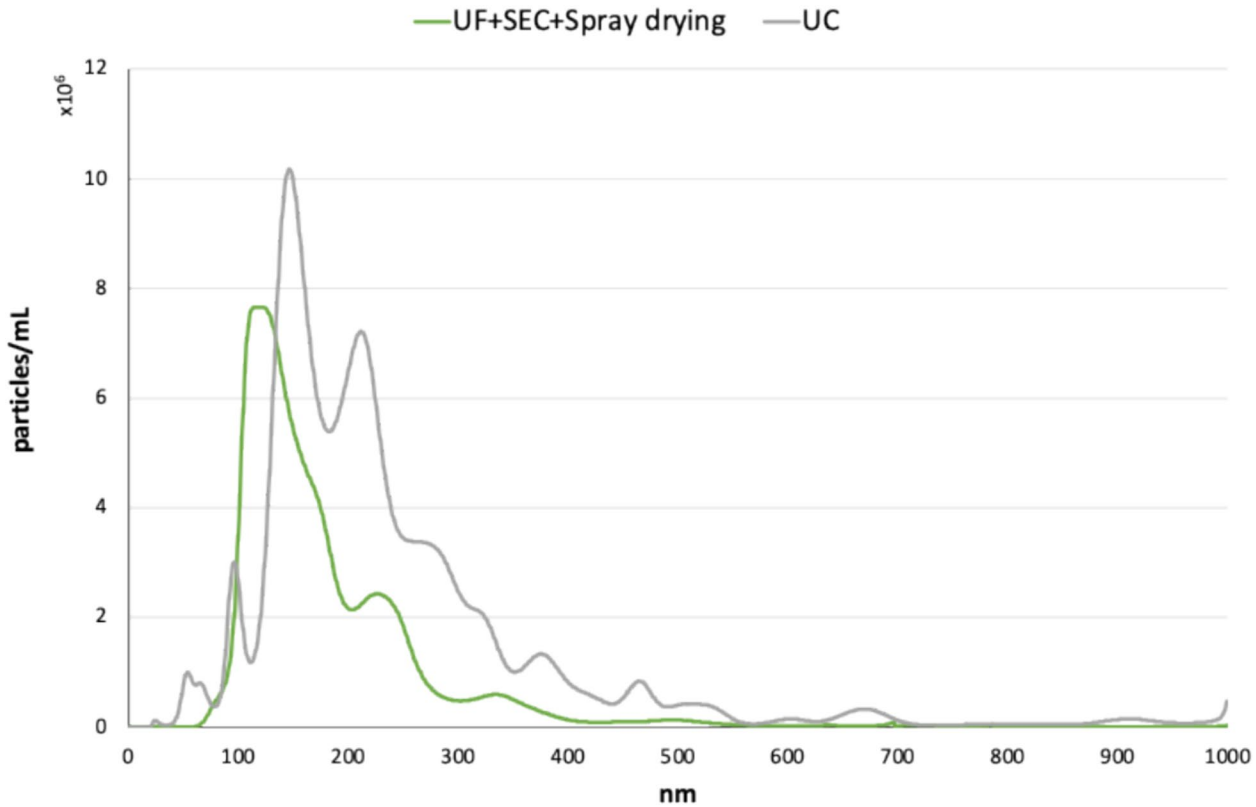

Fig. 1 NTA of ALVs obtained with different protocols. ALVs sample purified using UC (grey) and UF/SEC purification (green)

Table 1 Dynamic light scattering and nanoparticle tracking analysis results. results are expressed as the mean ± s.d. ($n = 3$)

Condition	DLS			NTA			
	Angle (°)	*D_h (nm)*	*PDI*	*D10 (nm)*	*D50 (nm)*	*D90 (nm)*	*Particles/mL*
-	173°	314 ± 117	0.724 ± 0.024	123 ± 8	204 ± 5	399 ± 17	$7.8\ (\pm 0.1) \times 10^{8}$
	12.8°	636 ± 23	0.873				
UC	173°	179 ± 16	0.756 ± 0.060	117 ± 20	170 ± 10	239 ± 20	$5.8\ (\pm 0.2) \times 10^{10}$
	12.8°	426 ± 7	0.142 ± 0.024				
UF + SEC	173°	138 ± 12	0.283 ± 0.224	104 ± 3	142 ± 2	218 ± 3	$1.9\ (\pm 0.8) \times 10^{7}$
	12.8°	-	-				
UF + SEC + Spray drying	173°	131 ± 11	0.431 ± 0.147	87 ± 2	122 ± 2	214 ± 2	$6.7\ (\pm 0.2) \times 10^{8*}$
	12.8°	-	-				

DLS Dynamic Light Scattering, *NTA* Nanoparticle Tracking Analysis, *D_h* Z-average diameter, *PDI* Polydispersity Index, *UC* Ultracentrifugation, *UF* Ultrafiltration, *SEC* Size exclusion chromatography

* Refers to 10 mg of ALVs powder solved in 1 mL of deionized water

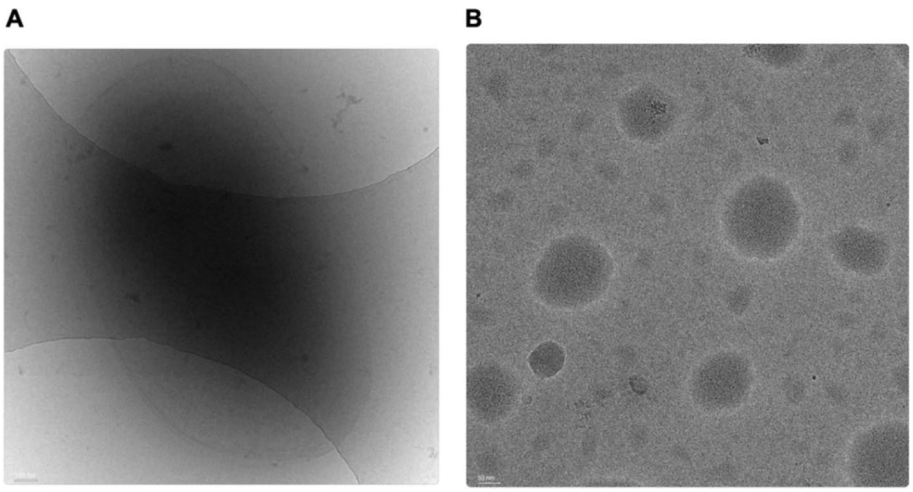

Fig. 2 Cryogenic electron microscopy, physico-chemical characterization and Raman spectra (200–2,500 cm − 1 region) of ALVs. **A** 0.5–2 µm structures with a sharp edge like a membrane. These objects are fully filled. Scale bar 100 nm. **B** 50–200 nm structures without sharp edge, likely lipidic drops/nanoemulsion. Scale bar 50 nm

the secondary structure of the proteins, circular dichroism (CD) spectra in the far-UV range (190–250 nm) were recorded (Fig. 3A). The spectra revealed one positive Cotton effect at 193 and two negative Cotton effects at 208 and 222 nm, indicative of the presence of α-helical proteins (Holzwarth & Doty, 1965), likely localized within the vesicle membrane layer. Further insights into the tertiary structure of ALV proteins were obtained through intrinsic fluorescence spectroscopy, a technique sensitive to the polarity of amino acid residues in the protein microenvironment (Vera et al., 2019). The analysis primarily detects tryptophan (Trp) and tyrosine (Tyr) residues, due to their high fluorescence quantum yield. Upon excitation at 280 nm, fluorescence spectra were recorded within the 310–450 nm range. ALVs showed a maximum fluorescence emission (λmax) at 330–332 nm (Fig. 3B). Based on λmax, Trp residues can be classified as (Burstein et al., 1973): (i) buried (λmax = 330–332 nm), (ii) partially exposed (λmax = 340–342 nm), or (iii) fully exposed (λmax = 350–353 nm). The observed λmax indicates that Trp residues are buried, suggesting that, in agreement with CD results, the alpha-helices are mainly localized in the vesicle membrane.

The biochemical fingerprint of ALVs was further analyzed by Raman spectroscopy. After baselines subtraction, the ALV mean spectrum (Fig. 3C) displayed characteristic bands corresponding to nucleic acids (720–828 cm^{-1}), phenylalanine (1,002 cm^{-1}), and lipid/protein markers, (CH and CH_2 groups at 1,450 cm^{-1}) (Movasaghi et al., 2007). Additional peaks at 883 cm^{-1} (protein), 1,084 cm^{-1} (phosphodiester groups in nucleic acids), and 1,337 cm^{-1} (protein and DNA) were also

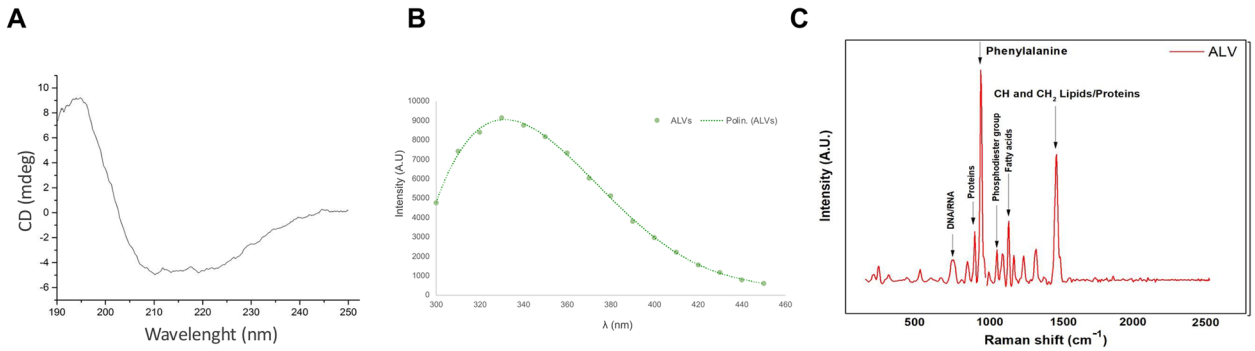

Fig. 3 Physico-chemical characterization of ALVs. **A** CD spectra of ALVs sample and (**B**) Intrinsic fluorescence signal detection of ALVs sample. **C** Raman spectra (200–2,500 cm^{-1} region) of ALV sample. Raman spectrum shows typical characteristic bands of nucleic acids, lipids and proteins, and a broad band of phenylalanine

detected (H. Zhang et al., 2020). These findings provide valuable insights into the molecular composition of ALVs and set the basis for subsequent metabolomic and transcriptomic analysis.

ALVs derived bioactive content identification

The chemical composition of ALVs was characterized using a metabolomic approach and miRNA sequencing, respectively. To isolate the vesicle cargo, ALVs were disrupted with ultrasonic waves, followed by centrifugation to separate the lipid external structure from the inner vesicular content. The resulting cargo composition was analyzed using Liquid Chromatography High-Resolution Mass Spectrometry (LC-HRMS). A total of 26 metabolites were identified, as summarized in Table 2, including their chemical class, molecular formula, and retention time. These metabolites were categorized into amino acids, fatty acids, polyphenols, carboxylic acids, and purine bases. The analysis amino acids detected included L-Leucine + L-Isoleucine, L-Arginine, L-Tryptophan, and L-Phenylalanine. Fatty acids such as linoleic acid, myristic acid and palmitoleic acid were also present. Carboxylic acids identified included succinic acids, L-malic acid, fumaric acid, 4-hydroxybenzaldehyde, salicylic acid, cinnamic acid, p-Coumaric acid, isoeugenol, gallic acid, citric acid, and ferulic acid. Among phenolic compounds salidroside, a glucosylated form of tyrosol) was found, along with flavonoids such as apigenin, astragalin and quercetin-3-O-glucoside. Furanoid lignans, including pinoresinol diglucoside and pinoresinol diglucoside + HCOOH, were also identified.

For qualitative characterization, the parameters adopted are the following: the result is green if the mass error is < 5 ppm, the library hit score is above 70%, and the Formula Finder score is above 50%. It is considered yellow if the mass error is < 10 ppm, the library hit score is above 50%, and the Formula Finder score is above 20%. Finally, it is red when the mass error is ≥ than 10 ppm, the library hit score is ≤ 50%, and the Formula Finder score is ≤ 20% (Table S2).

To analyse the miRNA content of ALVs, total RNA was extracted from 100 mg of ALV powder and subjected to miRNA sequencing. Sequencing results were aligned with the sequences of all known mature miRNAs to identify putative miRNAs. The identified miRNAs and the relative families are reported in Table 3.

In vitro ALVs bioavailability studies using differentiated human intestinal Caco-2 cells

Before conducting trans-epithelial transport experiments, the potential cytotoxic effects of ALVs on Caco-2 cells were assessed using the MTT assay. The results demonstrated that ALVs were non-toxic to human intestinal Caco-2 across the concentrations range 0.05–1 mg/mL (Fig. 4A), which correspond to the range 3.35—67×10^6 ALVs/mL.

To evaluate ALV transport across intestinal barrier, ALVs were labeled with MC540 (ALVs-MC540), and fluorescence was measured in basolateral (BL) solutions. After 2 and 4 h of incubation with ALVs-MC540 at a concentration of 0.5 mg/mL in the apical (AP) compartment, fluorescent signals were detected at 580 nm (excitation: 530 nm) in the BL. Results expressed as relative fluorescent units (RFU) (Fig. 4B), indicated time-dependent transport of ALVs-MC540 with RFU values of 222.981,00 ± 32% after 2 h and 673.671,00 ± 25% after 4 h. Quantitative analysis revealed that 26.6% of incubated ALVs-MC540 were found in BL solution after 4 h of incubation (Fig. 4C).

During the experiments, the integrity of the Caco-2 monolayer was monitored by measuring transepithelial electric resistance (TEER). TEER measurements (Fig. 4D) confirmed that the incubation of ALVs-MC540 on the AP side did not affect monolayer permeability, indicating the

Table 2 Secondary metabolite identified by HR-HPLC–MS

Component Name	Area	Retention Time (min)	Adduct/Charge	Formula	Precursor Mass	Found At Mass	Mass Error (ppm)	Library Hit	Library Score	Library Confidence
Aminoacids										
L-Leucine + L-Isoleucine	7.06E + 05	1.99	[M-H]-	C6H13NO2	130.0874	130.0874	0.7	L-Leucine + L-Isoleucine	64.5	Yellow
L-Arginine	1.12E + 05	1.02	[M-H]-	C6H14N4O2	173.1044	173.1043	−0.5	L-Arginine	81.8	Green
L-Tryptophan	5.83E + 06	5.57	[M-H]-	C11H12N2O2	203.0826	203.0825	−0.4	L-Tryptophan	100	Green
L-Phenylalanine	2.43E + 06	5.09	[M-H]-	C9H11NO2	164.0717	164.0717	0.2	L-Phenylalanine	98.5	Green
Fatty Acids										
Linoleic acid	3.80E + 05	11.62	[M-H]-	C18H32O2	279.233	279.2322	−2.6	Linoleic acid	99.5	Green
Myristic acid	6.23E + 04	11.29	[M-H]-	C14H28O2	227.2017	227.2014	−1.2	Myristic acid	97.2	Green
Palmitoleic acid	5.72E + 05	11.47	[M-H]-	C16H30O2	253.2173	253.2167	−2.3	Palmitoleic acid	100	Green
Purine base										
Guanosine	1.87E + 06	5.07	[M-H]-	C10H13N5O5	282.0844	282.0841	−1.1	Guanosine	100	Green
Polyphenols and Carboxylic acids										
Succinic acid	1.63E + 06	2.12	[M-H]-	C4H6O4	117.0193	117.0194	0.7	Succinic acid	100	Green
L-Malic acid	3.35E + 06	1.12	[M-H]-	C4H6O5	133.0142	133.0144	0.8	L-Malic acid	93.3	Green
Fumaric acid o maleic acid	1.74E + 06	1.12	[M-H]-	C4H4O4	115.0037	115.0038	0.8	Fumaric acid o maleic acid	98.6	Green
4-Hydroxybenzaldehyde	3.95E + 04	7.22	[M-H]-	C7H6O2	121.0295	121.0294	−0.9	4-Hydroxybenzaldehyde	94.2	Green
4-Hydroxybenzoic acid	5.07E + 05	6.09	[M-H]-	C7H6O3	137.0244	137.0245	0.6	4-Hydroxybenzoic acid	100	Green
Salicylic acid	5.07E + 05	6.09	[M-H]-	C7H6O3	137.0244	137.0245	0.6	Salicylic acid	99.2	Green
Cinnamic acid	7.02E + 05	5.08	[M-H]-	C9H8O2	147.0452	147.0452	0.2	Cinnamic acid	92.9	Green
p-Coumaric acid	8.68E + 04	6.36	[M-H]-	C9H8O3	163.0401	163.0398	−1.8	p-Coumaric acid	90.2	Green
Isoeugenol	2.49E + 05	8.27	[M-H]-	C10H12O2	163.0765	163.076	−2.6	Isoeugenol	82.1	Green
Gallic acid	5.28E + 04	3.51	[M-H]-	C7H6O5	169.0142	169.014	−1.3	Gallic acid	96.5	Green
Citric acid	3.42E + 07	1.56	[M-H]-	C6H8O7	191.0197	191.0199	0.8	Citric acid	97.7	Green
Ferulic acid	6.80E + 04	7.31	[M-H]-	C10H10O4	193.0506	193.0499	−3.6	Ferulic acid	96.8	Green
Apigenin	2.07E + 04	8.12	[M-H]-	C15H10O5	269.0455	269.0447	−3.2	Apigenin	55.1	Yellow
Salidroside	1.10E + 06	5.87	[M-H]-	C14H20O7	299.1136	299.1131	−1.9	Salidroside	94.8	Green
Astragalin	2.51E + 05	7.81	[M-H]-	C21H20O11	447.0933	447.0921	−2.6	Astragalin	97.3	Green
Quercetin-3-O-glucoside	3.37E + 04	6.61	[M-H]-	C21H20O12	463.0882	463.0883	0.3	Quercetin-3-O-glucoside	81.7	Green
Pinoresinol Diglucoside	6.00E + 04	6.95	[M-H]-	C32H42O16	681.24	681.2377	−3.3	Pinoresinol Diglucoside	78.5	Green
Pinoresinol Diglucoside + HCOOH	4.31E + 04	6.96	[M-H]-	C32H42O16.HCOOH	727.2455	727.2441	−1.9	Pinoresinol Diglucoside + HCOOH	90.5	Green

Table 3 List of the mature miRNAs detected in total RNA of ALVs by miRNA sequencing

miRNA family	Mature miRNAs
miR156	miR156a, miR156a.1, miR156a.2, miR156a.3, miR156b, miR156b-5p, miR156c, miR156d, miR156e, miR156f, miR156g, miR156h, miR156i, miR156j, miR156l, miR156m, miR156n, miR156o
miR157	miR157a, miR157a-5p, miR157b, miR157b.1, miR157b.2, miR157b.3, miR157b.4, miR157c, miR157d
miR158	miR158a, miR158b
miR159	miR159a, miR159b, miR159c, miR159d, miR159j, miR159k, miR159m, miR162, miR162b
miR165	miR165a, miR165b
miR166	miR166a, miR166a, miR166b, miR166b.1, miR166c, miR166c, miR166c.1, miR166c.2, miR166c.3, miR166c.4, miR166d, miR166d.1, miR166d.2, miR166d.3, miR166e, miR166f, miR166g, miR166h, miR166i, miR166j, miR166k, miR166l, miR166m, miR166n, miR166o, miR166p, miR166q, miR166r, miR166s, miR166t
miR167	miR167a, miR167b, miR167c, miR167d, miR167e, miR167f, miR167g, miR167h, miR167i, miR167j, miR167k, miR167l, miR167m, miR167n, miR167o, miR167p, miR167q, miR167r, miR167s, miR167t
miR319	miR319a, miR319a.1, miR319a.2, miR319b, miR319c, miR319d, miR319e, miR319f, miR319g, miR319h
miR390	miR390a, miR390a.1, miR390a.3, miR390a-5p, miR390b, miR390c, miR390d
miR394	miR394a, miR394a.1, miR394a.2, miR394a.3, miR394a.4, miR394a-5p, miR394b, miR394b-5p
miR403	miR403a, miR403b, miR403c, miR403d, miR403e, miR403f
miR408	miR408.1, miR408.2, miR408-5p, miR408b
Altri	miR168, miR2005, miR2910, miR2911, miR2914, miR395c, miR396b, miR398, miR4995, miR5368, miR59-npr, miRf10192-akr, miRf10258-akr, miRf10482-akr, miRf10804-akr, miRf12412-akr, miRf12524-akr, miR58-1-npr, miR58-2-npr, miR58-3-npr, miR21-1-npr, miR21-2-npr

safety of the sample for up to 4 h of exposure. In line with these results, morphological analysis by Confocal microscopy further supported these findings revealing intracellular red fluorescence signals in the cytoplasm of Caco-2 cells after 2 h of treatment (Fig. 4E). Notably, intracellular fluorescence appeared more pronounced at 8×10^6 ALVs/mL compared to 40×10^6 ALVs/mL, suggesting a concentration-dependent uptake of vesicles.

Discussion

ALVs production, stabilization and chemical characterization

This study has introduced an innovative bottom-up workflow using an integrated operational approach to isolate plant nanovesicle and plant lipid nanoparticle complexes. Traditionally, the most widely used approach to obtain plant-derived vesicles is based on differential ultracentrifugation (UC), a technique that separates, but does not purify, liquid sample components based on differences in density, size, and shape. UC involves high-speed centrifugal forces to sediment molecules at various rates, enabling the isolation of components from complex mixtures with heterogeneous profile (Chen et al., 2019). However, the primary limit of the time-consuming UC method, is that it produces fractions consisting of impure, aggregated PDVs with compromised structural integrity (Subha et al., 2023).

To address these limitations, we developed a tailored protocol utilizing UF coupled with SEC.

Our results demonstrate that this method efficiently generates, separates, and purifies plant vesicles and lipid nanoparticles from fresh arugula leaf homogenates. Unlike UC, UF-SEC is a more specific and versatile approach that is also industrially scalable and applicable to various food matrices (Sidhom et al., 2020). Comparative analysis showed that with UC can enrich ALV fractions, the degree of purification is significantly lower than UF-SEC, resulting in highly heterogenous and aggregated samples. Moreover, the high centrifugation forces applied during UC may compromise the structural integrity of ALVs.

Characterization by DLS, NTA, and Cryo-EM revealed that the ALVs obtained through our innovative technology are structurally intact, highly pure, and available in high quantities. These methods are straightforward to perform and offer reproducible results (Table 1 and Figs. 1–2). Cryo-EM analysis, which provides superior detail over TEM for examining EV morphology (Emelyanov et al., 2020), revealed two distinct vesicle populations: a minority of ectosome-like structures (0.5–2 μm), and a majority of 50–200 nm lipidic droplets (LDs). These smaller lipidic particles, with dimensions outside the typical range of endogenous plant LDs, likely form spontaneously during processing. Interestingly, nano-sized LDs have been shown to efficiently cross cell barriers (Khatri & Shao, 2017), protect against oxidative stress and lipotoxicity, (Zhao et al., 2022) and hold potential as self-nano-emulsifying drug delivery systems for the oral delivery of protein/peptide drugs (Wang et al., 2016). To stabilize the ALVs for practical use (e.g., formulation of food supplements and/or functional foods), a spray drying process was applied enabling long term storage while

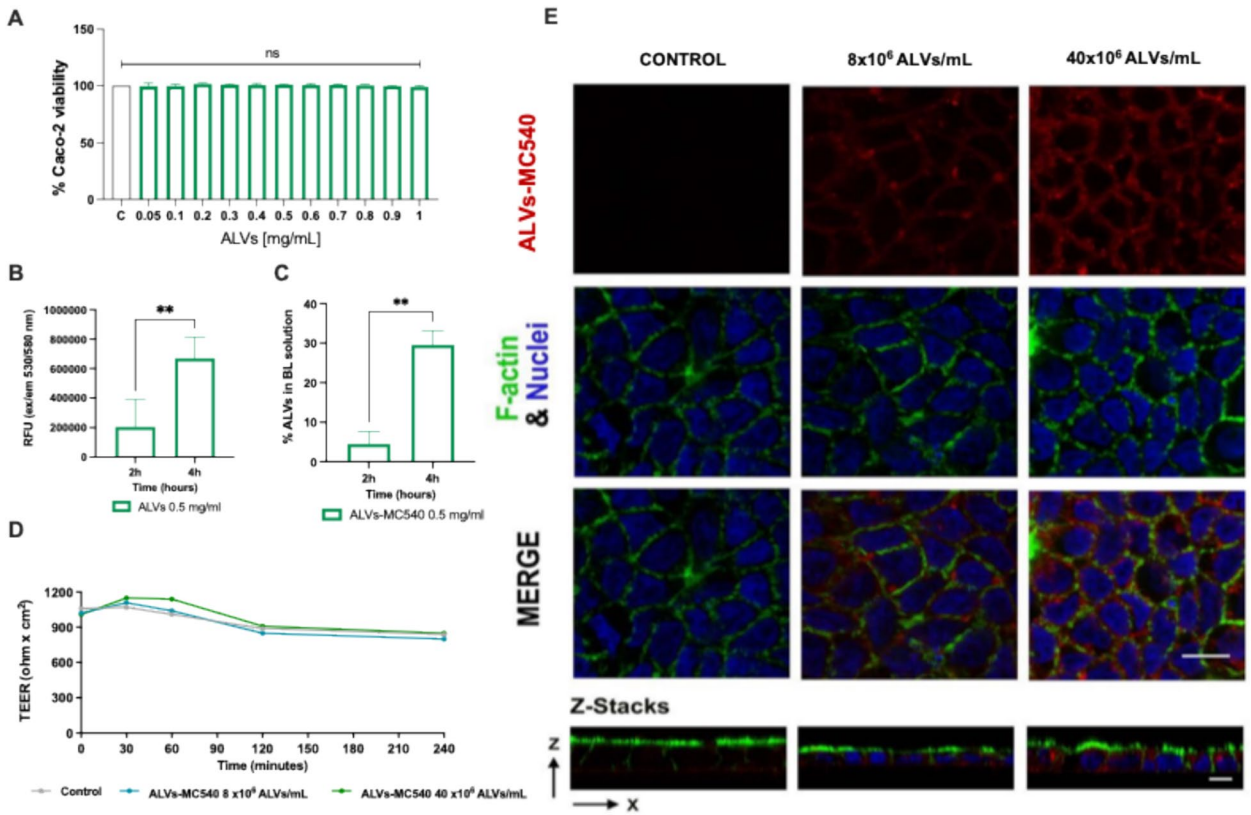

Fig. 4 Evaluation of ALVs effects on cellular viability, linear transport and intracellular localization of stained Arugula leaves derived nanovesicles (ALVs-MC540) in polarized Caco-2 cells. **A** Effect of ALVs on Caco-2 cells viability. **B** Relative fluorescence units (RFU) of basolateral solution after 2 and 4 h of ALVs-MC540 treatment (0.5 mg/mL). **C** Percentage of ALVs-MC540 detected in basolateral solution after 2 and 4 h of incubation. **D** Time course of TEER changes recorded in untreated (control), and ALVs-MC540 treated differentiated Caco-2 cells. **E** Intracellular localization of stained ALVs-MC540 in polarized Caco-2 cells. ALVs-MC540: red; nuclei, DAPI: blue; F-actin, FITC-conjugated phalloidin: green. Upper panel Single optical section (x–y) Z-Stacks: cross-sectional view of z-stack (z–y bottom panel). Scale bar 10 µm. Bars represent the mean ± s.d. of four independent experiments performed in triplicate. All data sets were analyzed by one-way ANOVA followed by Tukey's post hoc test. C: untreated cells. ns, not significant. ALVs [0.05 mg/mL] = 3.35×10^6 ALVs/mL. ALVs [0.1 mg/mL] = 6.7×10^6 ALVs/mL. ALVs [0.2 mg/mL] = 13.4×10^6 ALVs/mL. ALVs [0.3 mg/mL] = 20.1×10^6 ALVs/mL. ALVs [0.4 mg/mL] = 26.8×10^6 ALVs/mL. ALVs [0.5 mg/mL] = 33.5×10^6 ALVs/mL. ALVs [0.6 mg/mL] = 40.2×10^6 ALVs/mL. ALV [0.7 mg/mL] = 46.9×10^6 ALVs/mL. ALVs [0.8 mg/mL] = 53.6×10^6 ALVs/mL. ALVs [0.9 mg/mL] = 60.3×10^6 ALVs/mL. ALVs [1 mg/mL] = $67 \times 10.^6$ ALVs/mL. TEER = Trans-epithelial electrical resistance; ALVs-MC 540 = ALVs stained with Merocyanine Dye 540

preserving the vesicles' size, concentration and structural integrity. In this context, scarce literature evidence suggests that lyophilization has been applied upon UC process (J. Kim et al., 2022) (Table 1 and Fig. 1). Unlike freezing, which can damage vesicular membrane and cause consequent leakage (Bosch et al., 2016), spray drying is reproducible, affordable, quick, and easily scalable (Gatto & Najahi-Missaoui, 2023). This process resulted in a final product containing 67–78 million non-aggregated nanovesicles/mL, with neutral potential and diameters ranging between 50 nm and 2 µm.

Biochemical analysis using CD, intrinsic fluorescence, and Raman spectroscopy (Fig. 3) confirmed the presence of α-helical proteins and provided a detailed fingerprint of the ALVs (H. Zhang et al., 2020). Metabolomic analysis identified 26 secondary metabolites, including amino acids, fatty acids, polyphenols, carboxylic acids, and purine bases (Table 2). These compounds, consistent with the phytochemical profile of arugula leaves (Jin et al., 2009; Martínez-Sánchez et al., 2008), are known for their antioxidant, anti-inflammatory (Godlewska-Żyłkiewicz et al., 2020), anti-cancer, neuroprotective (Caruso et al., 2022), antimicrobial (Adamczak et al., 2020), and hypocholesterolemic activities (Cruz-Chamorro et al., 2023; Lammi et al., 2020). In addition, miRNA sequencing revealed 181 known plant miRNAs among 1736 sequences, with some highly enriched (e.g., mir165, miR166, miR167). Although the function of mammalian miRNAs has been widely investigated (Marangon et al., 2019, 2021) the cross-kingdom regulation of

plant-derived miRNAs in mammalian organisms is still in its infancy. Different plant miRNAs were detected in human plasma samples and human and porcine milk, following consumption of juice, vegetables, and fruits (Samad et al., 2021) Several reports suggested that after being acquired orally through the diet, plant miRNAs, encapsulated in nanovesicles, can survive in the digestive tract, enter the circulatory system, and regulate endogenous mRNAs (del Pozo-Acebo et al., 2021). For example, miR168a, a miRNA abundant in rice, was found highly enriched in the sera of Chinese subjects (L. Zhang et al., 2012). Functional studies in vitro and in vivo demonstrated that miR168a could bind to the human/mouse low-density lipoprotein receptor adapter protein 1 (LDLRAP1) mRNA, inhibit its expression in liver, and consequently decrease LDL removal from mouse plasma. Based on these findings, future studies will be addressed on assessing the potential effect that miRNAs enriched in ALVs could explicate on the mammalian genome, by applying target prediction and target validation approaches. It is worth mentioning that the illustrated method for isolating ALVs was not developed to ensure the integrity of the RNA content and that a lot of degraded ribosomal RNA was detected during the sequencing, thus reducing the depth of the analysis. Therefore, an optimization of the methodology that aims to protect RNA from degradation throughout the process will lead to better elucidating the landscape of miRNAs that characterize ALVs.

ALVs in vitro trans-epithelial transport

Literature data suggested that vesicles derived from different plant species (e.g. fruit juice (Raimondo et al., 2015), roots (Zhuang et al., 2015), leaves and seeds (Raimondo et al., 2015; Regente et al., 2009) have shown different therapeutic potential, mediated by their biological compound's cargo. Based on their chemical composition, it is reasonable to hypothesize that ALVs are intrinsically bioactive. Nevertheless, since bioavailability is a crucial step in the study of food derived bioactive compounds, they should be able to cross the intestinal barrier. To assess the ability of ALVs to be absorbed at intestinal level, human differentiated Caco-2 cells were employed and a dedicated protocol for the fluorescence labelling of ALVs was specifically developed. Results underlined that ALVs can be successfully transported by intestinal cells and comparing the fluorescence percentage of BL and AP solution, it emerges that the ALV absorption is time dependent, 26.6% of the vesicles in the apical chamber pass into the basolateral chamber after 4 h (Fig. 4C). Confocal microscopy analysis confirmed that fluorescent ALVs were absorbed by enterocytes in a dose-depended manner and that they successfully localize at intracellular level (Fig. 4E). The TEER results (Fig. 4D) were measured during the experiments and results indicated the ALVs did not negatively affect these values, suggesting that they are safe for the cell monolayer integrity and permeability. Further experiments are needed to elucidate the mechanism of action through which ALVs enter and cross the intestinal cells, but we hypothesize that transcytosis and/or phagocytosis may occur. ALVs did not alter the viability of treated human intestinal Caco-2 in the range of concentration 0.05–1 mg/mL (3.35×10^6 ALVs/mL—67×10^6 ALVs/mL) (Fig. 4A). These results are in line with recent data suggesting that lemon-derived vesicles are rich in citric acid and vitamin C and show a significant protective effect against oxidative stress in mesenchymal stem cells (Baldini et al., 2018); the prevention of oxidative stress was also observed in a dose-dependent manner on mesenchymal stem cells treated with strawberries derived vesicles (Perut et al., 2021). Literature evidence preliminary suggested that plant nanovesicles exert antioxidant activity in cellular and animal models, however the mechanism of action is poor investigated (Feng et al., 2023). The obtained results successfully addressed the primary aspect concerning the ability of ALVs to be transported by intestinal cells over time and in a dose-dependent manner, without compromising intestinal permeability and integrity.

Conclusion

This study introduces a versatile and environmentally friendly workflow for producing plant food nanovesicles. Due to their unique morphological, structural and functional characteristics, plant-derived nanovesicles represent a potential food ingredient for further application in food and nutraceutical sector. Doubtless, this study represents a first step to pave the way to this innovative research field, but further studies are necessary to investigate PDVs biological properties using cell-based assay, to obtain the evidence whether PDVs' bioactive cargo can reach the cell target where they can exhibit their bioactivities. Moreover, in vivo studies will be essential to establish the *proof of concept* for PDVs bioavailability and to confirm their potential health-promoting effects.

Abbreviations

ALVs	Arugula Leaves Vesicles
ALVs-MC540	ALVs stained with Merocyanine 540
CD	Circular Dichroism
COC	Cyclic Olefin Copolymer
Cryo-EM	Cryogenic Electron Microscopy
DAPI	4′,6-Diamidino-2-Phenylindole
DC	Differential Centrifugation
Dh	Z-Average Diameter
DLS	Dynamic Light Scattering
HCl	Hydrochloric Acid

HPLC	High-Performance Liquid Chromatography
ICG	Indocyanine Green
IP method	Innovative Patented Method
miRNA	MicroRNA
MTT	3-(4,5-Dimethylthiazol-2-yl)-2,5-Diphenyltetrazolium Bromide
NTA	Nanoparticle Tracking Analysis
PDI	Polydispersity Index
PDVs	Plant-Derived Nanovesicles
RFU	Relative Fluorescent Units

Supplementary Information

The online version contains supplementary material available at https://doi.org/10.1186/s43014-025-00353-w.

Supplementary Material 1. Table S3 NTA results on ALVs solution and spray-dried powder prepared on February 2nd, 2023, and analyzed after about 6 months on July 28th, 2023, and after 24 months on April 3rd, 2025.

Acknowledgements
The authors acknowledge "MIND FoodS HUB (Milano Innovation District Food System Hub): Innovative concept for the eco intensification of agricultural production and for the promotion of dietary patterns for human health and longevity through the creation in MIND of a digital Food System Hub", cofunded by POR FESR 2014 2020_BANDO Call HUB Ricerca e Innovazione, Regione Lombardia. We are indebted to Carlo Sirtori Foundation (Milan, Italy) for having provided part of equipment used in this experimentation. We acknowledge UNITECH OMICs, mass spectrometry platform of Università degli Studi di Milano, for running mass spectrometry analyses L.d'A. and D.M. acknowledge the PON "Ricerca e Innovazione" 2014-2020, Asse IV "Istruzione e ricerca per il recupero" con riferimento all'Azione IV.4 "Dottorati e contratti di ricerca su tematiche dell'innovazione" e all'Azione IV.5 "Dottorati su tematiche green". DM 1061/2021.

Patent
The method described in this paper, which includes ALVs isolation, purification and stabilization is referenced in the patent WO 2024/223549 A1 (Method for the production of plant-derived nanovesicles and their applications).

Authors' contributions
Conceptualization and Supervision: C.L.; Funding acquisition: C.L., D.L., L.S.; Investigation: L.d'A., U.M., D.M. D.L., G.R., G.F., A.L, C.M., B.L, R.P; Formal Analysis: L.d'A, C.L., A.L.C., B.L. Writing – original draft: L.d'A., D.M.; Writing – review: C.L., D.L, A.L.C, A.L., L.S., M.P.A.

Funding
No funding was received for this study.

Data availability
The data supporting the findings of this study are not publicly available due to confidentiality restrictions, as the research is subject to patent protection and involves proprietary information.

Declarations

Competing interests
The authors declare no conflicts of interest, except for patent n.PCT/WO 2024/223549 A1 "Method for the production of plant-derived nanovesicles and their applications", owned by Università degli Studi di Milano, which is directly related to the content of this publication. The authors declare that Patent n° PCT/WO 2024/223549 A1 "Method for the production of plant-derived nanovesicles and their applications", has been licensed to Plantech s.r.l., a company in which Carmen Lammi is a scientific director and co-founder.

Author details
[1]Department of Pharmaceutical Sciences, University of Milan, Milan, Italy. [2]Research Centre for Food and Nutrition, CREA, Rome, Italy. [3]Istituto Di Biologia E Biotecnologia Agraria, Consiglio Nazionale Delle Ricerche IBBA CNR, Milan 20122, Italy. [4]NeMO Lab, ASST GOM Niguarda Cà Granda Hospital, Milan 20162, Italy.

Received: 7 October 2025 Accepted: 2 November 2025
Published online: 13 February 2026

References

Adamczak, A., Ożarowski, M., & Karpiński, T. M. (2020). Antibacterial activity of some flavonoids and organic acids widely distributed in plants. *Journal of Clinical Medicine*. https://doi.org/10.3390/jcm9010109

Baldini, N., Torreggiani, E., Roncuzzi, L., Perut, F., Zini, N., & Avnet, S. (2018). Exosome-like nanovesicles isolated from *Citrus limon* L. exert antioxidative effect. *Current Pharmaceutical Biotechnology, 19*(11), 877–885. https://doi.org/10.2174/1389201019666181017115755

Bosch, S., De Beaurepaire, L., Allard, M., Mosser, M., Heichette, C., Chrétien, D., Jegou, D., & Bach, J. M. (2016). Trehalose prevents aggregation of exosomes and cryodamage. *Scientific Reports*. https://doi.org/10.1038/srep36162

Burstein, E. A., Vedenkina, N. S., & Ivkova, M. N. (1973). Fluorescence and the location of tryptophan residues in protein molecules. *Photochemistry and Photobiology*. https://doi.org/10.1111/j.1751-1097.1973.tb06422.x

Caruso, G., Godos, J., Privitera, A., Lanza, G., Castellano, S., Chillemi, A., Bruni, O., Ferri, R., Caraci, F., & Grosso, G. (2022). Phenolic acids and prevention of cognitive decline: Polyphenols with a neuroprotective role in cognitive disorders and Alzheimer's disease. *Nutrients*. https://doi.org/10.3390/nu14040819

Chen, B. Y., Sung, C. W. H., Chen, C., Cheng, C. M., Lin, D. P. C., Huang, C. T., & Hsu, M. Y. (2019). Advances in exosomes technology. *Clinica Chimica Acta*. https://doi.org/10.1016/j.cca.2019.02.021

Cruz-Chamorro, I., Santos-Sánchez, G., Ponce-España, E., Bollati, C., d'Adduzio, L., Bartolomei, M., Li, J., Carrillo-Vico, A., & Lammi, C. (2023). MOMAST® reduces the plasmatic lipid profile and oxidative stress and regulates cholesterol metabolism in a hypercholesterolemic mouse model: The proof of concept of a sustainable and innovative antioxidant and hypocholesterolemic ingredient. *Antioxidants*. https://doi.org/10.3390/antiox12071335

d'Adduzio, L., Fanzaga, M., Capriotti, A. L., Taglioni, E., Boschin, G., Laganà, A., Rueller, L., Robert, J., van Gemmern, A., Bollati, C., & Lammi, C. (2024). Ultrasonication coupled to enzymatic hydrolysis of soybean okara proteins for producing bioactive and bioavailable peptides. *Current Research in Food Science*. https://doi.org/10.1016/J.CRFS.2024.100919

del Pozo-Acebo, L., López de las Hazas, M. C., Margollés, A., Dávalos, A., & García-Ruiz, A. (2021). Eating microRNAs: pharmacological opportunities for cross-kingdom regulation and implications in host gene and gut microbiota modulation. *British Journal of Pharmacology*, *178*(11), 2218-2245. https://doi.org/10.1111/bph.15421

Emelyanov, A., Shtam, T., Kamyshinsky, R., Garaeva, L., Verlov, N., Miliukhina, I., Kudrevatykh, A., Gavrilov, G., Zabrodskaya, Y., Pchelina, S., & Konevega, A. (2020). Cryo-electron microscopy of extracellular vesicles from cerebrospinal fluid. *PLoS ONE*. https://doi.org/10.1371/journal.pone.0227949

Feng, J., Xiu, Q., Huang, Y., Troyer, Z., Li, B., & Zheng, L. (2023). Plant-derived vesicle-like nanoparticles as promising biotherapeutic tools: Present and future. *Advanced Materials*. https://doi.org/10.1002/adma.202207826

Ferruzza, S., Rossi, C., Sambuy, Y., & Scarino, M. L. (2013). Serum-reduced and serum-free media for differentiation of caco-2 cells. *Altex, 30*(2), 159–168. https://doi.org/10.14573/altex.2013.2.159

Gatto, M. S., & Najahi-Missaoui, W. (2023). Lyophilization of nanoparticles, does it really work? Overview of the current status and challenges. *International Journal of Molecular Sciences*. https://doi.org/10.3390/ijms241814041

Godlewska-żyłkiewicz, B., Świsłocka, R., Kalinowska, M., Golonko, A., Świderski, G., Arciszewska, Ż, Nalewajko-Sieliwoniuk, E., Naumowicz, M., & Lewandowski, W. (2020). Biologically active compounds of plants: Structure-related antioxidant, microbiological and cytotoxic activity of selected carboxylic acids. *Materials*. https://doi.org/10.3390/ma13194454

Holzwarth, G., & Doty, P. (1965). The ultraviolet circular dichroism of polypeptides. *Journal of the American Chemical Society*. https://doi.org/10.1021/ja01080a015

Jin, J., Koroleva, O. A., Gibson, T., Swanston, J., Maganj, J., Zhang, Y. A. N., Rowland, I. R., & Wagstaff, C. (2009). Analysis of phytochemical composition and chemoprotective capacity of rocket (Eruca sativa and Diplotaxis

tenuifolia) leafy salad following cultivation in different environments. *Journal of Agricultural and Food Chemistry*. https://doi.org/10.1021/jf9002973

Johnston, A. P. R., Such, G. K., Ng, S. L., & Caruso, F. (2011). Challenges facing colloidal delivery systems: From synthesis to the clinic. *Current Opinion in Colloid & Interface Science, 16*(3), 171–181. https://doi.org/10.1016/J.COCIS.2010.11.003

Kameli, N., Dragojlovic-kerkache, A., Savelkoul, P., & Stassen, F. R. (2021). Plant-derived extracellular vesicles: Current findings, challenges, and future applications. *Membranes, 11*(6), 411. https://doi.org/10.3390/MEMBRANES11060411

Khatri, P., & Shao, J. (2017). Transport of lipid nano-droplets through MDCK epithelial cell monolayer. *Colloids and Surfaces b: Biointerfaces, 153*, 237–243. https://doi.org/10.1016/j.colsurfb.2017.02.024

Kim, J., Lee, Y. H., Wang, J., Kim, Y. K., & Kwon, I. K. (2022). Isolation and characterization of ginseng-derived exosome-like nanoparticles with sucrose cushioning followed by ultracentrifugation. *SN Applied Sciences*. https://doi.org/10.1007/s42452-022-04943-y

Kim, S. Q., & Kim, K. H. (2022). Emergence of Edible Plant-Derived Nanovesicles as Functional Food Components and Nanocarriers for Therapeutics Delivery: Potentials in Human Health and Disease. Cells. 2022;11(14), 2232. https://doi.org/10.3390/CELLS11142232

Kolluru, L. P., Atre, P., & Rizvi, S. A. A. (2021). Characterization and Applications of Colloidal Systems as Versatile Drug Delivery Carriers for Parenteral Formulations. Pharmaceuticals. 2021;14(2), 108. https://doi.org/10.3390/PH14020108

Lammi, C., Aiello, G., Bollati, C., Li, J., Bartolomei, M., Ranaldi, G., Ferruzza, S., Fassi, E. M. A., Grazioso, G., Sambuy, Y., Sambuy, Y., & Arnoldi, A. (2021). Trans-epithelial transport, metabolism and biological activity assessment of the multi-target lupin peptide lilpkhsdad (P5) and its metabolite lpkhsdad (p5-met). *Nutrients, 13*(3), 1–17. https://doi.org/10.3390/nu13030863

Lammi, C., Bellumori, M., Cecchi, L., Bartolomei, M., Bollati, C., Clodoveo, M. L., Corbo, F., Arnoldi, A., & Mulinacci, N. (2020). Extra virgin olive oil phenol extracts exert hypocholesterolemic effects through the modulation of the LDLR pathway: In vitro and cellular mechanism of action elucidation. *Nutrients*. https://doi.org/10.3390/nu12061723

Magri, G., Franzé, S., Musazzi, U. M., Selmin, F., & Cilurzo, F. (2019). Maltodextrins as drying auxiliary agent for the preparation of easily resuspendable nanoparticles. *Journal of Drug Delivery Science and Technology, 50*(January), 181–187. https://doi.org/10.1016/j.jddst.2019.01.019

Marangon, D., Abbracchio, M. P., & Lecca, D. (2021). Pathway-focused profiling of oligodendrocytes over-expressing miR-125a-3p reveals alteration of Wnt and cell-to-cell signaling. *Cellular and Molecular Neurobiology*. https://doi.org/10.1007/s10571-020-00836-z

Marangon, D., Raffaele, S., Fumagalli, M., & Lecca, D. (2019). Micrornas change the games in central nervous system pharmacology. *Biochemical Pharmacology*. https://doi.org/10.1016/j.bcp.2019.06.019

Martínez-Sánchez, A., Gil-Izquierdo, A., Gil, M. I., & Ferreres, F. (2008). A comparative study of flavonoid compounds, vitamin C, and antioxidant properties of baby leaf Brassicaceae species. *Journal of Agricultural and Food Chemistry*. https://doi.org/10.1021/jf072975+

Movasaghi, Z., Rehman, S., & Rehman, I. U. (2007). Raman spectroscopy of biological tissues. *Applied Spectroscopy Reviews*. https://doi.org/10.1080/05704920701551530

Natoli, M., Leoni, B. D., D'Agnano, I., Zucco, F., & Felsani, A. (2012). Good Caco-2 cell culture practices. *Toxicology in Vitro*. https://doi.org/10.1016/j.tiv.2012.03.009

Ortega-Hernández, E., Antunes-Ricardo, M., & Jacobo-Velázquez, D. A. (2021). Improving the health-benefits of kales (*Brassica oleracea* L. var. *acephala* DC) through the application of controlled abiotic stresses: A review. *Plants, 10*(12), 2629. https://doi.org/10.3390/PLANTS10122629

Perut, F., Roncuzzi, L., Avnet, S., Massa, A., Zini, N., Sabbadini, S., Giampieri, F., Mezzetti, B., & Baldini, N. (2021). Strawberry-derived exosome-like nanoparticles prevent oxidative stress in human mesenchymal stromal cells. *Biomolecules*. https://doi.org/10.3390/biom11010087

Raimondo, S., Naselli, F., Fontana, S., Monteleone, F., Lo Dico, A., Saieva, L., Zito, G., Flugy, A., Manno, M., Di Bella, M. A., De Leo, G., & Alessandro, R. (2015). *Citrus limon*-derived nanovesicles inhibit cancer cell proliferation and suppress CML xenograft growth by inducing TRAIL-mediated cell death. *Oncotarget*. https://doi.org/10.18632/oncotarget.4004

Regente, M., Corti-Monzón, G., Maldonado, A. M., Pinedo, M., Jorrín, J., & de la Canal, L. (2009). Vesicular fractions of sunflower apoplastic fluids are associated with potential exosome marker proteins. *FEBS Letters*. https://doi.org/10.1016/j.febslet.2009.09.041

Rome, S. (2019). Biological properties of plant-derived extracellular vesicles. *Food & Function, 10*(2), 529–538. https://doi.org/10.1039/C8FO02295J

Samad, A. F. A., Kamaroddin, M. F., & Sajad, M. (2021). Cross-kingdom regulation by plant microRNAs provides novel insight into gene regulation. *Advances in Nutrition*. https://doi.org/10.1093/advances/nmaa095

Sidhom, K., Obi, P. O., & Saleem, A. (2020). A review of exosomal isolation methods: Is size exclusion chromatography the best option? *International Journal of Molecular Sciences, 21*(18), 1–19. https://doi.org/10.3390/ijms21186466

Simon A. (2020). Babraham Bioinformatics - FastQC A Quality Control tool for High Throughput Sequence Data. In *Soil*.

Subha, D., Harshnii, K., Madhikiruba, K. G., Nandhini, M., & Tamilselvi, K. S. (2023). Plant derived exosome- like nanovesicles: An updated overview. *Plant Nano Biology*. https://doi.org/10.1016/j.plana.2022.100022

Tan, Y., & McClements, D. J. (2021). Plant-based colloidal delivery systems for bioactives. Molecules 2021;26(22):6895. https://doi.org/10.3390/MOLECULES26226895

Vera, A., Valenzuela, M. A., Yazdani-Pedram, M., Tapia, C., & Abugoch, L. (2019). Conformational and physicochemical properties of quinoa proteins affected by different conditions of high-intensity ultrasound treatments. *Ultrasonics Sonochemistry*. https://doi.org/10.1016/j.ultsonch.2018.10.026

Wang, Y., Zhou, X. M., Ma, X., Du, Y., Zheng, L., & Liu, P. (2016). Construction of nanodroplet/adiposome and artificial lipid droplets. *ACS Nano, 10*(3), 3312–3322. https://doi.org/10.1021/acsnano.5b06852

Yi, X., Zhang, Z., Ling, Y., Xu, W., & Su, Z. (2015). PNRD: A plant non-coding RNA database. *Nucleic Acids Research*, *43*(D1), D982–D989. https://doi.org/10.1093/nar/gku1162

Zhang, H., Silva, A. C., Zhang, W., Rutigliano, H., & Zhou, A. (2020). Raman spectroscopy characterization extracellular vesicles from bovine placenta and peripheral blood mononuclear cells. *PLoS ONE*. https://doi.org/10.1371/journal.pone.0235214

Zhang, L., Hou, D., Chen, X., Li, D., Zhu, L., Zhang, Y., Li, J., Bian, Z., Liang, X., Cai, X., Yin, Y., Wang, C., Zhang, T., Zhu, D., Zhang, D., Xu, J., Chen, Q., Ba, Y., Liu, J., … Zhang, C. Y. (2012). Exogenous plant MIR168a specifically targets mammalian LDLRAP1: Evidence of cross-kingdom regulation by microRNA. *Cell Research*. https://doi.org/10.1038/cr.2011.158

Zhao, P., Jin, Y., Wu, X., Huang, J., Chen, L., Tan, Y., Yuan, H., Wu, J., & Ren, Z. (2022). Artificial lipid droplets: Novel effective biomaterials to protect cells against oxidative stress and lipotoxicity. *Nanomaterials (Basel), 12*(4), 1–17. https://doi.org/10.3390/nano12040672

Zhuang, X., Deng, Z. B., Mu, J., Zhang, L., Yan, J., Miller, D., Feng, W., McClain, C. J., & Zhang, H. G. (2015). Ginger-derived nanoparticles protect against alcohol-induced liver damage. *Journal of Extracellular Vesicles*. https://doi.org/10.3402/jev.v4.28713

Publisher's Note